First ZnGa2O4 transparent ceramics

Claire Mével, Julie Carreaud, Gaëlle Delaizir, Jean-René Duclère, François
Brisset, Julie Bourret, Pierre Carles, Cécile Genevois, Mathieu Allix,
Sébastien Chenu

Journal Pre-proof

First ZnGa$_2$O$_4$ Transparent Ceramics

Claire Mével, Julie Carreaud, Gaëlle Delaizir, Jean-René Duclère, François Brisset, Julie Bourret, Pierre Carles, Cécile Genevois, Mathieu Allix, Sébastien Chenu

First ZnGa₂O₄ Transparent Ceramics.

Claire Mével[1], Julie Carreaud[1], Gaëlle Delaizir[1], Jean-René Duclère[1], François Brisset[2], Julie Bourret[1], Pierre Carles[1], Cécile Genevois[3], Mathieu Allix[3], Sébastien Chenu[1]*

1- Institut de Recherche sur les Céramiques (IRCER), UMR 7315 CNRS, Université de Limoges, Centre Européen de la Céramique, Limoges, France

2 - Institut de Chimie Moléculaire et des Matériaux d'Orsay (ICMMO), UMR 8182 CNRS, Orsay, France

3- CNRS, Conditions Extrêmes et Matériaux : Haute Température et Irradiation (CEMHTI) UPR3079, Univ. Orléans, F-45071 Orléans, France

*Corresponding author: sebastien.chenu@unilim.fr

Abstract

Transparent polycrystalline ZnGa₂O₄ ceramics are synthesized, for the first time, by combining high-energy ball milling, solid-state reaction and spark plasma sintering. They appear transparent in both the visible and near infrared (up to 9 μm) ranges after a post-SPS annealing in air converting the raw semiconductor into an electrical insulator. The maximum of transmittance is reached in the near infrared region, at around 2.5 μm, with a value of 78 % (1 mm thick sample) close to the maximum value of transmittance previously measured for single crystals. These transparent ceramics present a classic cubic spinel ZnGa₂O₄ structure and a dense microstructure (> 99 %) attained without sintering aids, with an average grain size of 600 nm and a random orientation of the crystallites. TEM observations performed on thin foils have revealed limited nanometer scale intergranular porosity which does not affect much the transparency. As a proof of interest, red long-lasting luminescence arising from the entire sample volume is observed in these Cr³⁺ doped transparent ceramics. This innovative work is anticipated to further drive the development of transparent ZnGa₂O₄ ceramics towards a wider range of performing optical applications such as laser emission.

1

1. Introduction

The zinc gallate spinel ($ZnGa_2O_4$) has been widely studied for optical applications such as flat panel displays,[1, 2] saturable absorbers,[3] in vivo bio-imaging applications,[4-6] thermal sensors,[7, 8] X-ray dosimetry,[9] optoelectronics,[10, 11] anti-counterfeiting applications.[8, 12, 13] $ZnGa_2O_4$ crystallizes in a cubic direct "AB_2O_4" spinel structure with the $Fd\bar{3}m$ space group in which Zn^{2+} ions occupy the tetrahedral A-sites and Ga^{3+} the octahedral B-sites.[14] It can exhibit different emission colors when doped with transition metal elements.[1, 15-17] For example, when doped with Ni^{2+}, a broadband infrared luminescence emission is observed around 1300nm,[18, 19] while when doped with Cr^{3+}, it gives rise to an long red afterglow.[16, 20] Moreover, the long-lasting red luminescence properties of these spinel materials are shown to be much improved when germanium or tin are substituted to the nominal composition, leading to a $Zn_{1+x}Ga_{2-2x}Ge_xO_4$ solid solution.[21, 22] In recent years, much attention has been devoted to the zinc gallate spinel elaboration procedure to access specific optical applications. Over time, various synthesis methods emerged: after solid-state chemistry used to produce microcrystals powder,[23, 24] soft-chemistry methods were employed for synthesizing nanoparticles [6, 25, 26] or chemical deposition for thin films.[11, 27] In these cases, the spinel elaboration routes yield opaque polycrystalline ceramic materials preventing any volume effect as only the surface of the material is active for optical applications. Therefore, recent research activity has been focused on the study of transparent materials based on the zinc gallate spinel. Transparent silicate-based glass-ceramics containing $ZnGa_2O_4$ nanocrystals have been designed by inducing and controlling glass-glass phase separation in the glass precursor material which was further partially crystallized into

2

transparent glass-ceramics presenting red long lasting luminescence properties with a volume effect.[18, 28] More recently, similar silicate-based compositions doped with Mn^{2+} have been drawn into glass-ceramic fibers which are sensitive to pressure fluctuations.[8] If zinc gallate single crystal fibers have been elaborated by laser heating some time ago,[29, 30] in 2019 bulk $ZnGa_2O_4$ single crystals with ultra-wide bandgap were obtained directly by crystallization from the melt using the vertical gradient freeze and the Czochralski methods.[31]

Transparent polycrystalline ceramics have recently proved their potential for various optical applications as laser hosts, infrared lenses, transparent armors.[32, 33] These ceramics are characterized by their relatively shaping easiness, low cost elaboration, wide range of chemical compositions and the possibility to be heavily and homogenously doped.[34] Different processes can be used to elaborate transparent ceramics: in some cases, when the vitrification of the composition is achievable, transparent ceramics could be synthesized by a full crystallization process.[35-38] However, most transparent oxide ceramics are generally prepared from raw nanopowders or/and cubic crystalline powders through different sintering techniques (vacuum sintering, spark plasma sintering, hot uniaxial sintering).[34, 39, 40] Numerous studies report transparent spinel ceramics such as $MgAl_2O_4$[33, 41, 42] or $ZnAl_2O_4$[43-48] while the zinc gallate spinel has not been yet achieved as a transparent ceramic. Indeed, the difference of evaporation speed of ZnO and Ga_2O_3 (i.e. higher for Ga_2O_3) [31] leading to a stoichiometry deviation of spinel ceramics compositions and therefore the materials are opaque. Moreover, the unavailability of $ZnGa_2O_4$ commercial nanopowders could explain the absence of transparent $ZnGa_2O_4$ ceramics in the literature. Therefore, raw materials must be designed to develop such transparent ceramics.

2. Experimental Section
2.1 Powder Synthesis

3

The powder precursors mixture was prepared using high energy ball milling of high purity nanometric precursors (ZnO - Aldrich 99.99 %, Ga_2O_3 - NanoShel 99.9 %), with a RETSCH EMAX grinding machine. A 12 g batch was prepared in a 1:1 molar ratio, using a two-step grinding protocol. The batch was poured in a 125 ml zirconia-coated jar filled with ethanol and 500 μm diameter zirconia grinding beads. A 20 minutes ball milling duration was processed at 1700 rpm. After the separation of beads and suspension using a 63 μm sieve and the drying of the obtained suspension, a second grinding was made with 100 μm diameter zirconia beads using the same previous conditions. The separation of beads and precursor powder was made using a 32 μm sieve. Particle size of the powders has been estimated by laser granulometry, as illustrated in Figure SI-1. The powders of precursors exhibit a multimodal size distribution while after high energy ball milling process, the size distribution (grains in suspension) shows a single mode centered at 126 nm (with a median diameter d_{50} estimated at 116 nm). After drying, the precursors mixture was divided into two batches. A first undoped-batch was fired at 700°C for 2 h to remove volatile compounds, hydroxyl and carbonate species. The second Cr^{3+}-doped batch was first calcined at 500°C for 2 h, then mixed with 0.1 %$_{at}$ Cr^{3+} (Cr_2O_3 - Alfa Aesar 99.97 %) in an agate mortar with ethanol to ensure homogeneous repartition of dopant and finally fired at 700°C for 2 h. Both undoped and Cr^{3+}-doped powders were then considered ready for spark plasma sintering.

2.2 SPS sintering.

A Spark Plasma Sintering equipment (Dr. Sinter 825 Syntex machine (Fuji FDC, Japan)) was used to densify the precursor mixture previously obtained. To do so, the powder was poured into an 8 mm diameter graphite die. For all the SPS attempts, the temperature was measured with a thermocouple positioned close to the sample, through the die. The sintering was performed under vacuum and no sintering aids or additives were used. The temperature was increased to 450°C within 5 minutes without applying pressure, except for contact. A 5

4

minute dwell time was done while some uniaxial pressure of 100 MPa were applied. This pressure remained constant until the end of the run. At the end of the dwell time, the temperature was increased to higher temperatures (to 950°C) at a 100°C/min heating rate. The temperature was kept increasing at a 2°C/min heating rate until the sample displacement dropped. The run was stopped and the cooling was left free down to room temperature. The SPS sintering cycle and the associated displacement of matrix pistons are presented in **Figure SI-2**.

2.3 Characterization methods

Particle size analysis was performed by laser diffraction granulometry (Malvern Mastersizer 2000). The powder was dispersed in ethanol water by sonication for 5 min.

XRPD data were recorded on a Bragg Brentano D8 Advance Bruker diffractometer (CuKα radiation) equipped with a LynxEye XE detector over an angular range of $10° < 2\theta < 70°$ for phase identification and of $5° < 2\theta < 130°$ using a 0.012 step size for structural refinements. These latter were performed using the Rietveld [49] method implemented in the JANA2006 software.[50]

Electron backscatter diffraction (EBSD) maps were recorded on the ceramic materials using an OIM TSL/EDAX system mounted on a FEG-SEM (Zeiss SUPRA 55 VP) system in order to visualize the microstructure of sample without chemical or thermal etching and also to confirm the absence of amorphous parts in the ceramic materials. The samples were optically mirror-polished prior to observations.

Transmission Electron Microscopy (TEM) was used to characterize the nanostructure of the ceramic. High-resolution transmission electron microscopy (HRTEM), selected-area electron diffraction (SAED), and high-resolution scanning transmission electron microscopy – high angle annular dark field (HRSTEM-HAADF) were performed on a JEOL ARM 200F (JEOL Ltd.) colf FEG operating at 200 kV and equipped with a double spherical correctors.

5

Elemental maps were acquired by STEM-EDS using a JEOL SDD CENTURIO EDS system and a 0.13 nm probe size. The ceramics were prepared prior to (S)TEM observations by focused ion beam (FIB, ZEISS Crossbeam 550).

Optical transmission measurements were carried out within the 300 - 3300 nm range, with the sample placed at normal incidence, using a Varian Cary 5000 spectrophotometer operated in a dual beam configuration and in the infrared range using a Thermo Scientific Nicolet 6700. Photoluminescence (PL), as well as long lasting phosphorescence (LLP) measurements, were carried out at room temperature, using a Fluorolog 3 spectrofluorimeter from Horiba Jobin-Yvon company. For the recorded steady state fluorescence emission spectra, the data step was fixed to 0.25 nm, with a 0.5 s acquisition time and a 0.5 nm emission slit size. For the phosphorescence measurements, the delay time was fixed at 2 s, with a sample window of 0.5 s: the data step was fixed to 0.5 nm, with a 1 nm emission slit size. LLP data were collected 10 s after the excitation stoppage and then with time interval steps of 10 s. The afterglow intensity is normalized at 1 by using the value measured 10 s after the excitation stoppage, thus allowing the comparison of the rate of decay between the different curves.

3. Results and discussion

Herein, we report the elaboration and characterizations of the first $ZnGa_2O_4$ transparent ceramics. Stoichiometric amounts of commercial ZnO and Ga_2O_3 powders were finely ground in ethanol by high-energy ball milling process in zirconia media. The mixture was then calcined at 700°C for 2 h to remove volatile compounds, hydroxyl and carbonate species formed during the milling process. During this heat treatment, precursors reacted together to form the spinel ceramic. These powders were densified by spark plasma sintering (SPS) as described in the experimental section. The formation of $ZnGa_2O_4$ phase was totally completed during this SPS process. **Figure 1** shows the visual aspect of a $ZnGa_2O_4$ ceramic sintered by

6

SPS at a maximum temperature of 960 °C and optically polished (1 mm thickness). The ceramic appears transparent in the visible range and one can read the text through the polished sample which attests a limited light scattering effect in the material. To gain more information regarding this aspect, the transmittance has been measured by spectrophotometry (Figure 1). After post-SPS annealing in air during 4 hours at 800°C, the ceramic transmits light in the range from 0.4 to 9 μm. It can be noted that multiphonon cut-off of this ceramic is shifted towards higher wavelengths compared to other spinel ceramics such as $ZnAl_2O_4$ (7.8 μm) [48] or $MgAl_2O_4$ (6.3 μm) [51] due to the presence of elements with higher molar mass (i.e. Al is replaced by Ga).
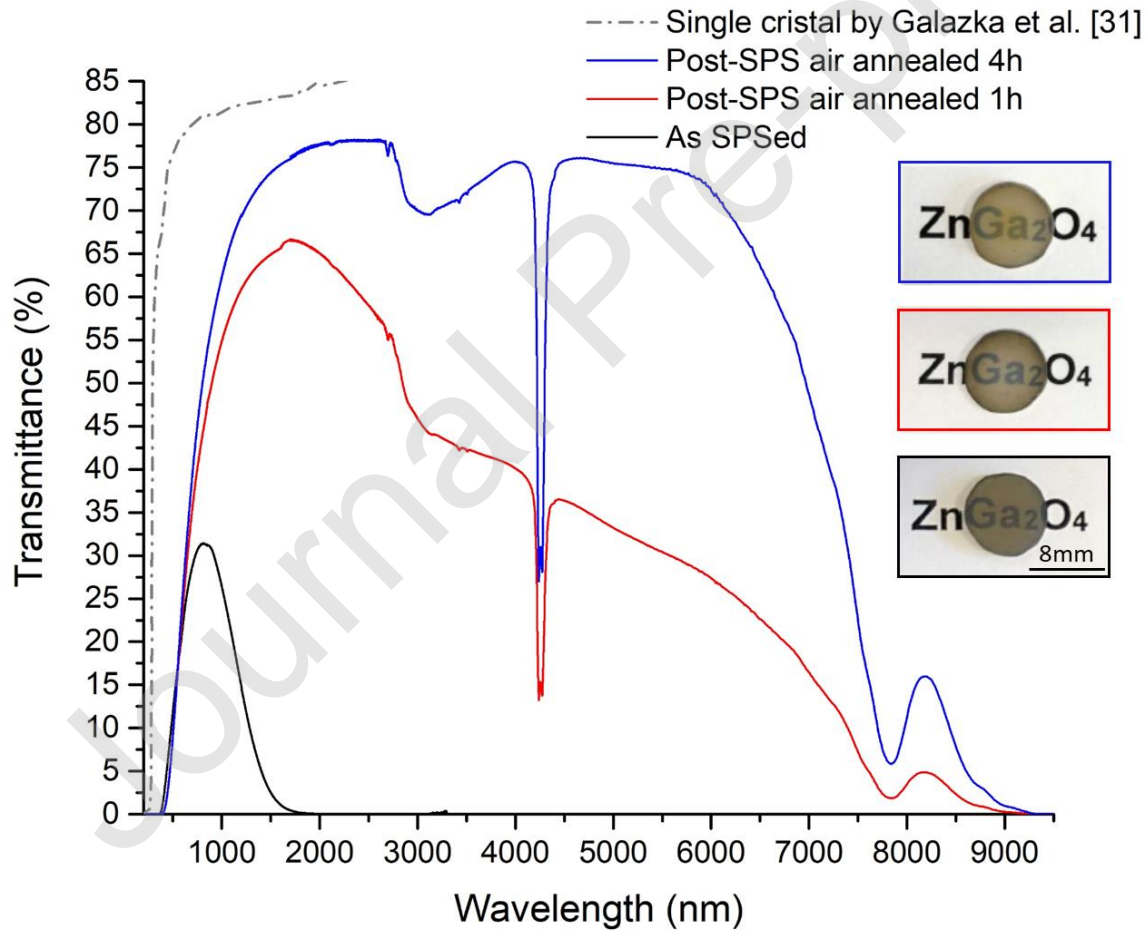

Figure 1: Optical transmittance spectra of $ZnGa_2O_4$ transparent ceramics densified by spark plasma sintering (black curve) and after post-SPS air annealing at 800°C during 1 and 4 hours in air (red and blue curves respectively). Photographs of the corresponding ceramics are also shown (thickness = 1 mm). The light transmission of a $ZnGa_2O_4$ single crystal, reported by

Galazka et al. [31] (dashed grey line) are also shown for comparison (0.25 ≤ thickness ≤ 0.5 mm). A sharp absorption band around 4.27 μm is observed and could be related to trapped CO_2 gazes.

Such an extended transparency window appears to be in agreement with the relative low phonon energy of this oxide ceramic which has already been evidenced by Raman spectroscopy. [52] The maximum of transmittance is reached in the near infrared region, around 2.5 μm, with a value of 78%. The limit of transmission at 2 μm has been measured recently on a $ZnGa_2O_4$ single crystal. This value is close to 82.5 %, which corresponds to a material with a linear refractive index of 1.90 .[31] The small differences between our $ZnGa_2O_4$ transparent ceramics and the transmittance measured on single crystal [31] suggest the presence of some limited scattering centers in our ceramics. For the same reasons, the transmission light for the ceramic is red-shifted compared to single crystal one. For example, a weak residual porosity, as well as the presence of small amounts of secondary phases, could lead to local birefringence effects, which would decrease the material transparency. [41, 53] Single phase spinel materials should indeed present optical isotropy given their cubic symmetry.[48]

To better understand this transmittance difference, the chromatic dependence of the $ZnGa_2O_4$ refractive index was measured by spectroscopic ellipsometry on a one-side polished ceramic sample (**Figure SI-3**). Using the well-known Sellmeier dispersion expression, it was also possible to correctly fit the refractive index data in the 250-1800 nm wavelength range. This allowed the extraction of the refractive index at infinite wavelength (where there is no more chromatic dispersion), which was found close to 1.89 ± 0.01. This value is in excellent agreement with the literature (1.90).[31] In the same way, the value of the band gap (Eg) was also estimated from the ellipsometry measurements, according to the UV absorption edge. Knowing the chromatic dependence of the extinction index k and as a consequence that of the absorption coefficient α, the Tauc plot was generated (**Figure SI-4**), in the case of a direct

transition allowed.[31] For this spinel $ZnGa_2O_4$ ceramic, the value of Eg is found to be about 4.82 ± 0.05 eV, which again falls in rather good agreement with E. Chikoidze et al.[10], where the authors reported that Eg was about 4.6 eV.

Thus, the maximum of 78 % reached experimentally is so far pretty good, but there is still some room for improvement. It is important to note than no sintering aids nor additives were used to enhance the optical transmittance. It is well known that sintering additives (such as ZnF_2 or LiF) could be employed to facilitate the shrinkage of the sample and to reduce the porosity during sintering procedures but also leads to significant grain growth and decreased mechanical properties.[33, 44]

Moreover, in the transparency range of $ZnGa_2O_4$ ceramics, two absorption bands are present in Figure 1. The broad one located around 3 μm is due to the presence of free hydroxyl groups [54] probably exacerbated by the milling procedure conducted in ethanol media. A second sharp absorption band around 4.27 μm is observed and could be related to CO_2 trapped in pores. Indeed, this band (at 2348 cm^{-1}) has already reported for $Lu_2Ti_2O_7$ pyrochlore [55] and $MgAl_2O_4$ spinel [56] materials, densified by SPS and post-SPS air annealed, due to the graphitic environment of this equipment. This phenomenon indicates the presence of porosity, source of light scattering.

The transmittance curve measured for the as-sintered $ZnGa_2O_4$ and polished ceramic (so without post-SPS annealing treatment) is quite surprising. As shown in Figure 1, the sample reveals a correct transmission in the visible spectrum which is concomitant with the associated photography of this ceramic while a significant drop is observed from 1.1 μm and beyond 2 μm, where no light is transmitted. In fact, such a behavior has been previously observed for $ZnGa_2O_4$ single crystals and attributed to semiconducting effects due to free carriers absorption (free electrons concentration at the level of 10^{18} cm^{-3}).[31, 57]

After post-SPS air annealing at 800°C during 4 hours, the ceramic switches into an electrically insulating state and becomes transparent until mid-infrared range (up to 9 μm) as

previously observed for same composition single crystals. [31] Besides, when compared to the undoped samples, it is worth mentioning that the optical transparency of Cr^{3+}-doped $ZnGa_2O_4$ ceramics seems similarly impacted by the heat treatment (**Figure SI-5**).

Furthermore, the greyish color observed for all these ceramics is probably due, in major part, to a small carbon contamination inherent to spark plasma sintering as extensively described in the literature.[58-60] The heat treatment apparently leads to a slight discoloration; the latter thus likely ascribed to the reduction of the carbon amount and/or the decrease of the oxygen vacancies concentrations.[40, 56] Moreover, no significant degradation of the transmittance in the visible range were noted for ceramics, which implies that no pore size evolution during this controlled post-treatment in air at 800°C.

For all these combined reasons (presence of residual carbon, pores and oxygen vacancies), the UV transmission edge measured for the ceramic (~ 0.4 μm) is clearly red-shifted compared to that of the single crystal, as illustrated in Figure 1.[31]

Obviously, providing a full explanation for the slight limitation of transmittance of this transparent ceramic requires some more complete structural and microstructural investigations.
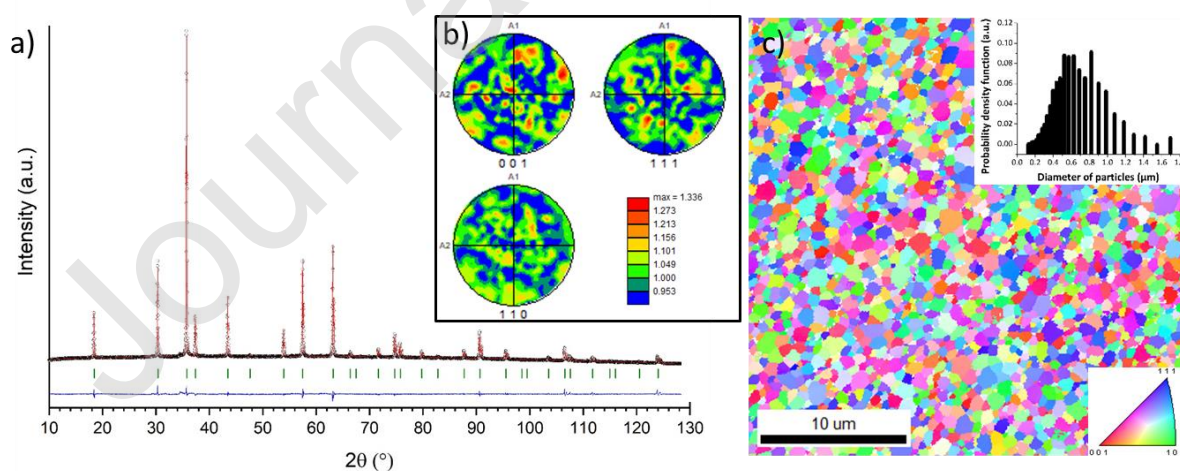

Figure 2: (a) Rietveld refinement plot from room temperature laboratory X-ray powder diffraction data recorded from a ground transparent $ZnGa_2O_4$ ceramic. Black circles, red and blue solid lines, vertical green ticks correspond to experimental data, simulated diagram, difference curve and indexations, respectively. Reliability factors are wRP = 2.75%, Rp =

1.80% and GOF = 2.05. A minor peak is observed at 32.4° due to K-beta radiation of X-rays sources attesting the high counting statistics. (b) Pole figures showing microstructure and texture in $ZnGa_2O_4$ ceramic. (c) EBSD-SEM map of the ceramic showing crystalline domains. Their size distribution is shown in insert.

As presented in **Figure 2-a**, the X-ray powder diffraction pattern of the $ZnGa_2O_4$ transparent ceramic obtained after the SPS process presents an excellent match with the known cubic spinel $ZnGa_2O_4$ structure (PDF 00-038-1240). No secondary crystalline phase was detected, within the accuracy of X-ray diffraction technique. The Rietveld refinement converged easily and the cell parameter a = 8.32151(3) Å is very close to the literature (8.3336 Å).[31] The refined XRPD data (agreement factors wRP=2.75 %, Rp = 1.80% and GOF = 2.05) are presented in Figure 2-a, and the resulting atomic positions of $ZnGa_2O_4$ are summarized in **Table SI-1**. The X-ray powder diffraction patterns of the material at different steps of the elaboration process are presented on **Figure SI-6**.

To gain more information regarding the transparency of this spinel ceramic, the microstructure of the SPS densified ceramic has been studied. Electron backscatter diffraction (EBSD) maps were recorded on the $ZnGa_2O_4$ ceramic (**Figure 2-c**). The crystalline domains show random orientations as illustrated by pole figures (**Figure 2-b**) and their size evolves from 100 nm to 1.8 μm with an average crystalline domains size around 700 nm. The absence of black (non-indexed) areas attests the high crystallinity of the ceramic and confirms the absence of glass phase and microscopic pores at grain boundary.

To gain insights regarding the nanometer scale microstructure, transmission electronic microscopy (TEM) characterizations have been performed on the ceramic samples.
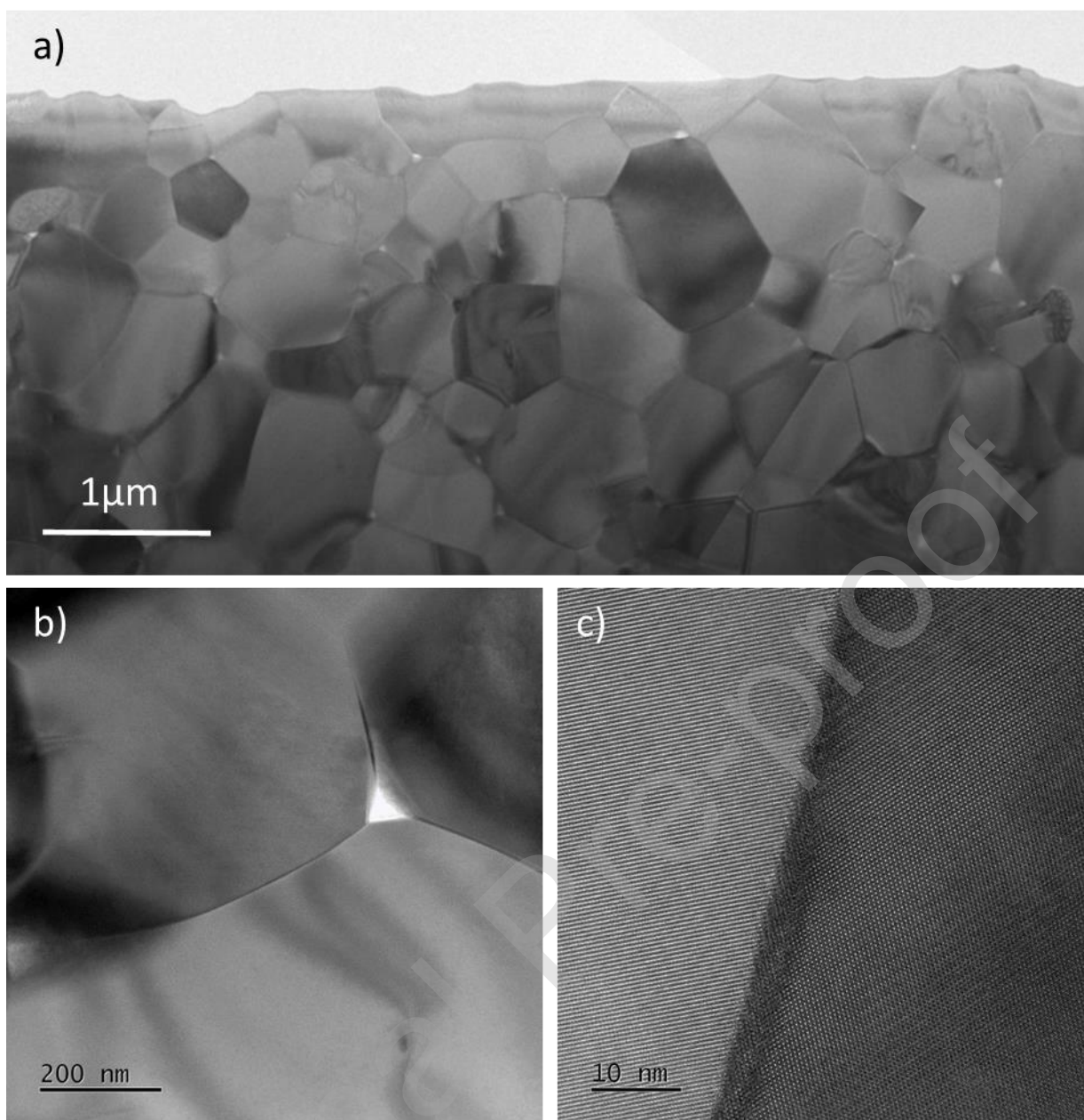
Figure 3: Cr^{3+}-doped $ZnGa_2O_4$ ceramic. (a) bright field TEM micrograph. (b) bright Field TEM observation of porosity at a grain boundary triple junction. (c) HRSTEM-HAADF of a thin grain boundary.

One can note that the nanostructure of our $ZnGa_2O_4$ transparent ceramic is composed of large number of crystalline angular shape grains with an average size of 560 nm (**Figure 3-a** and **Figure SI-7a**), in agreement with EBSD observations. A few grains are slightly larger and their size reaches 2 μm. Furthermore, TEM observations show the presence of nanometer scale porosity, which implies light scattering effect. This porosity appears only at grain boundaries (**Figure 3-b**). The average diameter of these intergranular pores is around 50 nm,

as illustrated for a grain boundary triple junction in Figure 3-b, therefore the possible deleterious effect on the light transmission is limited due to their relative small size (around one tens of the incident wavelength) according to the Rayleigh scattering law.[41] Moreover, the HRTEM images (**Figure SI-7c** and **Figure 3-c**) clearly show that the grain boundaries are very thin with no amorphous phase. No chemical segregations at the grain boundaries have been observed by STEM-EDS experiments (**Figure SI-7d**). Nevertheless, one can note the presence of a few grains with irregular shape (**Figure 3-a**). The red arrow points out one of these grains and corresponding STEM-EDX elemental maps have been recorded in this area (**Figure SI-7b**). The formation of a Zn-enriched secondary phase with segregation of zirconium (inferior to $2\%_{at}$) is observed. One can note that this secondary phase is not detected by XRD measurements attesting their very limited presence. The zirconium element is only detected in this secondary phase and derived from the milling procedure realized in zirconia media. These local observations (i.e. the presence of porosity and a small content of secondary phase) could explain the slight difference of transmittance between the measurements of our transparent ceramic and the one of the single crystal.[31] In order to evaluate the optical performance of this new transparent ceramic, photoluminescence (PL) measurements of a Cr^{3+}-doped ceramic were carried out.
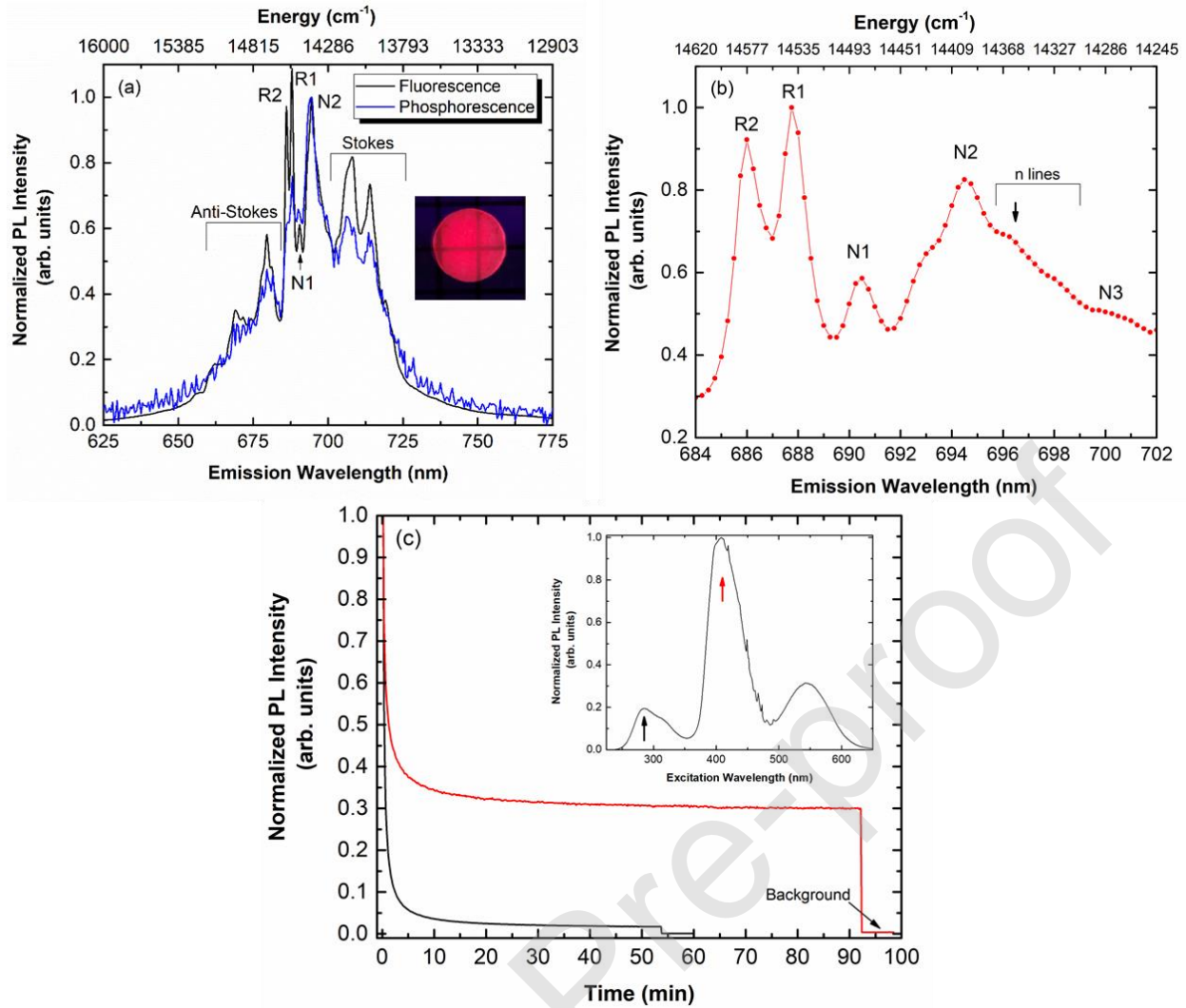
13

Figure 4: a) Photoluminescence (fluorescence and phosphorescence) spectra of Cr^{3+}-doped $ZnGa_2O_4$ ceramic densified by spark plasma sintering and post-SPS treated at 800°C during 4 hours. The excitation wavelength (λ_{exc}) used was 285 nm. The normalization to 1 is made on the N2 line, after background removal. A photograph of the corresponding materials, under UV light, is also shown attesting the typical red luminescence of this material. (Thickness = 1 mm). b) Zoom in the zero phonon line region (684 - 702 nm). PL data were collected for λ_{exc} = 410 nm. The normalization to 1 is made on the R1 line, after background removal. c) Normalized afterglow intensity recorded for λ_{em} = 694 nm (N2 line) as a function of time, for excitations fixed at 285 nm and 410 nm (black and red curves, respectively). The background originates from the electronic noise level of the detector and is simply evidenced by closing the shutter. Insert: Excitation spectrum of the samples associated to the emission at 694 nm. The employed excitation wavelengths in this study (285 and 410 nm) are respectively highlighted by the black and red arrows.

Since the work of Bessière *et al.*, it is well known that $ZnGa_2O_3$:Cr^{3+} materials are interesting red long-lasting phosphors, showing some high brightness. [16] First, under the 254 nm excitation of a commercial UV lamp, the Cr^{3+}-doped ceramic exhibits some red emission (see insert of **Figure 4-a**). In addition, the steady-state fluorescence data, displayed on Figure 4-a,

reveal that the luminescence is centered around ~ 694 nm (position of the N2 line° – see further), and also that the emission spectrum appears very similar to previous PL spectra collected for $ZnGa_2O_4$:Cr^{3+} powdered samples [16, 21, 61] or for transparent glass-ceramics containing $ZnGa_2O_4$:Cr^{3+} nanocrystals.[28] Zero-phonon R2 and R1 lines are respectively observed at 686 and 688 nm, corresponding to the ^2E (first excited state) → $^4A_2$ (ground state) electronic transitions of Cr^{3+} ions occupying the octahedral sites of an ideal spinel structure.[16, 62] Moreover, the weak trigonal distortion, combined to spin orbit coupling, leads to the splitting of the 2E level into two sub-levels separated by 40 cm^{-1},[63] which further give rise to the two R lines. R lines are also accompanied with the phonon side bands, which are located at the expected positions and labelled Stokes and Anti-Stokes on Figure 4-a. An additional PL feature is observed at ~ 694 nm, corresponding to the so-called N2 line. Such band was established to originate from another type of Cr^{3+} ions with a perturbed short-range crystalline order. Such perturbation corresponds to some environment distorted by an antisite defect, located in the first cationic neighbours of Cr^{3+} ions. [62, 64, 65]

A zoom in the Zero Phonon Line (ZPL) region of the ^2E → $^4A_2$ transition (684 – 702 nm range), provided on **Figure 4-b** for one of the two different excitation wavelengths (λ_{exc} = 410 nm) employed for the long lasting photoluminescence (LLP) experiments, helps to discuss the potential presence of other types of defects in the final material. First, the N1 line is clearly visible at ~ 690 nm. When looking at the literature, the explanations for such feature appear controversial. Effectively, the N1 line was for instance attributed to a Cr^{3+} - V_{Zn} pair (V_{zn} being a Zn vacancy), based on the work of Nie et al.[66] or to a Cr^{3+} - Zn_i pair (Zn_i being an interstitial Zn), according to Zhang et al.*[62]* Interestingly, considering the STEM-EDX maps, the formation of a Zn-enriched secondary phase has been evidenced in small quantity, which would then be more in favour of the formation of Cr^{3+} - Zn_i pairs. However, at this stage of our expertise on such Cr^{3+}-doped spinel ceramics, that conclusion remains impossible to draw. Besides, despite the post-annealing treatment under air during 4h at 800°C, oxygen

15

vacancies could obviously remain in the ceramic and their potential presence might be also considered in order to fully elucidate the PL features. On another hand, the N3 line, which is located around 700 nm, was unambiguously assigned to Cr^{3+} - Cr^{3+} pairs.[67, 68] One can definitely see in Figure 4-b that such type of defects is only present in traces in the final spinel ceramic, as the corresponding amplitude is almost negligible. Finally, both PL spectra in Figure 4-b display additional emissions labelled n lines. [61] Among these lines, one specific feature located at ~ 696 nm is highlighted by the black arrow: that one could be similar to the n8 line, which was attributed by Walsh et al.[69] to Cr^{3+} ions in gallium oxide (β-Ga_2O_3). However, neither XRD nor TEM data have revealed that there were any traces of Ga_2O_3 left. Long lasting luminescence (LLP) experiments were as well conducted on the Cr^{3+}-doped $ZnGa_2O_4$ ceramic. Before commenting on the LLP decays, it is important to mention that instead of recording LLP spectra, phosphorescence measurements were actually conducted. In fact, for us, it was the best compromise in order to detect some PL signal sufficiently high (*i.e.* without too much noise), and simultaneously maintain a good resolution for the acquisition (details are provided in the experimental section). Thus, on Figure 4-a, it can be clearly seen that the emission spectrum in phosphorescence mode is now characterized predominantly by the N2 line, as the intensity for the R lines strongly drops down. Indeed, it is well known that Cr^{3+} ions located at undistorted octahedral sites show very little LLP, whereas Cr^{3+} ions at distorted octahedral sites are related to an intense delayed emission. [16] In our configuration, undoubtedly, such mechanism is already at play, even just 2s after the excitation stoppage (value fixed for the delay time in our set-up – see experimental section). Normalized LLP decays are represented in **Figure 4-c**, for two different excitation wavelengths: namely 285 and 410 nm. One can easily notice that probing the ceramic sample with a 410 nm excitation (*i.e.* deeply within the band gap of $ZnGa_2O_4$) seems more efficient in terms of persistency of the light emission than to excite at 285 nm (energy much closer to that of the bang gap). Reasons for such pronounced differences are still under investigation, but stronger scattering

and/or absorption effects probably occur at 285 nm (in comparison with the excitation at 410 nm), leading to a reduced irradiated volume. As well, using the 410 nm excitation wavelength will very likely be more efficient to probe the luminescence of defects, for which the corresponding energy levels are localized deeply within the band gap. In addition, the PL excitation spectrum, for a fixed $\lambda_{em} = 694$ nm, is provided in the inset of Figure 4-c. Three broad absorption bands at around 285 nm, 410 nm and 545 nm, belonging to the $^4A_2(^4F)$ - $^4T_1(^4P)$, $^4A_2(^4F)$ - $^4T_1(^4F)$ and $^4A_2(^4F)$ - $^4T_2(^4F)$ Cr^{3+} d–d transitions, respectively, can be observed. This is in good agreement with what has been previously published for instance by Basavaraju *et al*. [70] However, even though the photon flux is limited below 250 nm for our equipment, the excitation band characteristic of the host material, normally located at ~ 245 nm according to Basavaraju et al.[70], appears to be absent. Based on the optical transmittance data (Figure 1), we know for the final ceramic that strong scattering and/or absorption effects occur in the UV. Finally, the afterglow intensity recorded at 694 nm as a function of time reveals that the red emission is still considerably higher than the background level, even more than 1.5 h after the excitation stoppage (for the excitation at 410 nm), thus attesting promising LLP properties.

4. Conclusion

The foregoing results highlight the possibility to obtain new highly transparent $ZnGa_2O_4$ ceramics by combining high energy milling of commercial powders of zinc and gallium oxides and SPS sintering. The resulting ceramic is transparent in both the visible and near infrared range (up to 9 μm) after a post-SPS annealing in air to convert it from a semiconductor to an electrical insulator. The maximum of transmittance is reached in the near infrared region around 2.5 μm with a value of 78 % (1 mm thick sample), close to the maximum value of transmittance previously measured for single crystals (82.5%).[31] Local TEM observations have revealed the presence of nanometric intergranular pores and a really

17

small content of secondary phase which can explain the slight difference of transmittance

compared to the single crystal. Red long-lasting luminescence arising from the sample volume

is observed in the Cr^{3+} doped transparent ceramics and confirmed the remarkable

performances of this material. Taking into account the simple fabrication process and optical

properties, these polycrystalline transparent $ZnGa_2O_4$ ceramics are believed to be promising

candidates for further use in wide optical applications such as lenses, saturable absorbers and

phosphor converters for high-power white-light LED and infrared laser.

Author Information
Corresponding author
*Email for S.C.: sebastien.chenu@unilim.fr

ORCID
Sébastien CHENU: 0000-0002-5648-9779

Notes
The authors declare no competing financial interest.

References

[1] T. Minami, Y. Kuroi, T. Miyata, H. Yamada, S. Takata, $ZnGa_2O_4$ as host material for multicolor-emitting phosphor layer of electroluminescent devices, J. Lumin. 72–74(0) (1997) 997-998.

[2] D. Hebbar N, K.S. Choudhari, N. Pathak, S.A. Shivashankar, S.D. Kulkarni, Rapid annealing-transformed, intense-red-emitting Eu-doped $ZnGa_2O_4$ nanoparticles with high colour purity, for very-high-resolution display applications, Mater. Res. Bull. 119 (2019) 110544.

[3] P.A. Loiko, O.S. Dymshits, N.A. Skoptsov, A.M. Malyarevich, A.A. Zhilin, I.P. Alekseeva, M.Y. Tsenter, K.V. Bogdanov, X. Mateos, K.V. Yumashev, Crystallization and nonlinear optical properties of transparent glass-ceramics with $Co:Mg(Al,Ga)_2O_4$ nanocrystals for saturable absorbers of lasers at 1.6–1.7μm, J. Phys. Chem. Solids 103 (2017) 132-141.

[4] T. Maldiney, A. Bessière, J. Seguin, E. Teston, S.K. Sharma, B. Viana, A.J.J. Bos, P. Dorenbos, M. Bessodes, D. Gourier, D. Scherman, C. Richard, The in vivo activation of persistent nanophosphors for optical imaging of vascularization, tumours and grafted cells, Nat Mater 13(4) (2014) 418-426.

[5] J. Nie, Y. Li, S. Liu, Q. Chen, Q. Xu, J. Qiu, Tunable long persistent luminescence in the second near-infrared window via crystal field control, Scientific Reports 7(1) (2017) 12392.

[6] M.N. Da Silva, J.M. De Carvalho, M.C. De Abreu Fantini, L.A. Chiavacci, C. Bourgaux, Nanosized $ZnGa_2O_4:Cr^{3+}$ Spinels as Highly Luminescent Materials for Bioimaging, Applied Nano Materials (2019).

[7] E. Glais, M. Pellerin, V. Castaing, D. Alloyeau, N. Touati, B. Viana, C. Chanéac, Luminescence properties of $ZnGa_2O_4:Cr^{3+},Bi^{3+}$ nanophosphors for thermometry applications, RSC Advances 8(73) (2018) 41767-41774.

19

[8] S. Lv, B. Shanmugavelu, Y. Wang, Q. Mao, Y. Zhao, Y. Yu, J. Hao, Q. Zhang, J. Qiu, S. Zhou, Transition Metal Doped Smart Glass with Pressure and Temperature Sensitive Luminescence, Advanced Optical Materials 6(21) (2018) 1800881.

[9] A. Luchechko, Y. Zhydachevskyy, S. Ubizskii, O. Kravets, A.I. Popov, U. Rogulis, E. Elsts, E. Bulur, A. Suchocki, Afterglow, TL and OSL properties of Mn^{2+}doped $ZnGa_2O_4$ phosphor, Scientific Reports 9(1) (2019) 9544.

[10] E. Chikoidze, C. Sartel, I. Madaci, H. Mohamed, C. Vilar, B. Ballesteros, F. Belarre, E. del Corro, P. Vales-Castro, G. Sauthier, L. Li, M. Jennings, V. Sallet, Y. Dumont, A. Pérez-Tomás, p-Type Ultrawide-Band-Gap Spinel $ZnGa_2O_4$: New Perspectives for Energy Electronics, Crystal Growth & Design (2020).

[11] Y.-C. Shen, C.-Y. Tung, C.-Y. Huang, Y.-C. Lin, Y.-G. Lin, R.-H. Horng, Study on Optoelectronic Characteristics of $ZnGa_2O_4$ Thin-Film Phototransistors, ACS Applied Electronic Materials 1(5) (2019) 783-788.

[12] C. Ma, H. Liu, F. Ren, Z. Liu, Q. Sun, C. Zhao, Z. Li, The Second Near-Infrared Window Persistent Luminescence for Anti-Counterfeiting Application, Crystal Growth & Design 20(3) (2020) 1859-1867.

[13] M.I. Chen, A.K. Singh, J.L. Chiang, R.H. Horng, D.S. Wuu, Zinc Gallium Oxide-A Review from Synthesis to Applications, Nanomaterials (Basel, Switzerland) 10(11) (2020).

[14] R.J. Hill, J.R. Craig, G.V. Gibbs, Systematics of the spinel structure type, Phys. Chem. Miner. 4(4) (1979) 317-339.

[15] H.-J. Byun, J.-U. Kim, H. Yang, Blue, green, and red emission from undoped and doped $ZnGa_2O_4$ colloidal nanocrystals, Nanotechnology 20(49) (2009) 495602.

[16] A. Bessiere, S. Jacquart, K. Priolkar, A. Lecointre, B. Viana, D. Gourier, $ZnGa_2O_4$:Cr^{3+}: a new red long-lasting phosphor with high brightness, Opt. Express 19(11) (2011) 10131-10137.

[17] Z. Gu, F. Liu, X. Li, J. Howe, J. Xu, Y. Zhao, Z. Pan, Red, Green, and Blue Luminescence from $ZnGa_2O_4$ Nanowire Arrays, The Journal of Physical Chemistry Letters 1(1) (2010) 354-357.

[18] S. Chenu, E. Véron, C. Genevois, G. Matzen, T. Cardinal, A. Etienne, D. Massiot, M. Allix, Tuneable Nanostructuring of Highly Transparent Zinc Gallogermanate Glasses and Glass-Ceramics, Advanced Optical Materials 2(4) (2014) 364-372.

[19] Z. Gao, Y. Liu, J. Ren, Z. Fang, X. Lu, E. Lewis, G. Farrell, J. Yang, P. Wang, Selective doping of Ni^{2+} in highly transparent glass-ceramics containing nano-spinels $ZnGa_2O_4$ and $Zn_{(1+x)}Ga_{(2-2x)}Ge_xO_4$ for broadband near-infrared fiber amplifiers, Scientific Reports 7 (2017) 1783.

[20] P. Dhak, U.K. Gayen, S. Mishra, P. Pramanik, A. Roy, Optical emission spectra of chromium doped nanocrystalline zinc gallate, J. Appl. Phys. 106(6) (2009).

[21] M. Allix, S. Chenu, E. Véron, T. Poumeyrol, E.A. Kouadri-Boudjelthia, S. Alahraché, F. Porcher, D. Massiot, F. Fayon, Considerable Improvement of Long-Persistent Luminescence in Germanium and Tin Substituted $ZnGa_2O_4$, Chem. Mater. 25(9) (2013) 1600-1606.

[22] Z.W. Pan, Y.Y. Lu, F. Liu, Sunlight-activated long-persistent luminescence in the near-infrared from Cr^{3+}-doped zinc gallogermanates, Nature Materials 11(1) (2012) 58-63.

[23] K.H. Hsu, M.R. Yang, K.S. Chen, A study of $ZnGa_2O_4$ phosphor prepared by the solid method, Journal of Materials Science-Materials in Electronics 9(4) (1998) 283-288.

[24] K. Uheda, T. Maruyama, H. Takizawa, T. Endo, Synthesis and long-period phosphorescence of $ZnGa_2O_4$: Mn^{2+} spinel, J. Alloys Compd. 262 (1997) 60-64.

[25] Z. Li, Y. Zhang, X. Wu, L. Huang, D. Li, W. Fan, G. Han, Direct Aqueous-Phase Synthesis of Sub-10 nm "Luminous Pearls" with Enhanced in Vivo Renewable Near-Infrared Persistent Luminescence, J. Am. Chem. Soc. 137(16) (2015) 5304-5307.

[26] H.S. Roh, Y.C. Kang, S.B. Park, H.D. Park, $ZnGa_2O_4$: Mn phosphor particles with spherical shape and clean surface, Japanese Journal of Applied Physics 41(7A) (2002) 4559-4562.

[27] I.J. Hsieh, K.T. Chu, C.F. Yu, M.S. Feng, Cathodoluminescent characteristic of $ZnGa_2O_4$ phosphor grown by radio-frequency magnetron sputtering, J. Appl. Phys. 76(6) (1994) 3735-3739.

[28] S. Chenu, E. Veron, C. Genevois, G. Alain, G. Matzen, M. Allix, Long-lasting luminescent $ZnGa_2O_4$:Cr^{3+} transparent glass-ceramics, Journal of Materials Chemistry C 2 (2014) 10002-10010.

[29] N.F. Santos, A.J.S. Fernandes, L.C. Alves, N.A. Sobolev, E. Alves, K. Lorenz, F.M. Costa, T. Monteiro, Microprobe analysis, iono- and photo-luminescence of Mn^{2+} activated $ZnGa_2O_4$ fibres, Nuclear Instruments and Methods in Physics Research Section B: Beam Interactions with Materials and Atoms 306 (2013) 195-200.

[30] W. Jia, H. Liu, S. Huang, X. Wu, L. Lu, W.M. Yen, Photoluminescence of Mn^{2+} - Doped $ZnGa_2O_4$ Single‐Crystal Fibers, J. Electrochem. Soc. 142(5) (1995) 1637-1640.

[31] Z. Galazka, S. Ganschow, R. Schewski, K. Irmscher, D. Klimm, A. Kwasniewski, M. Pietsch, A. Fiedler, I. Schulze-Jonack, M. Albrecht, T. Schröder, M. Bickermann, Ultra-wide bandgap, conductive, high mobility, and high quality melt-grown bulk $ZnGa_2O_4$ single crystals, APL Materials 7(2) (2019) 022512.

[32] R. Won, Ceramic future, Nature Photonics 2(4) (2008) 216-217.

[33] S. Maxim, R. Barak, K. Sergey, D.M. Peter, G. Ehud, F. Nachum, Transparent Polycrystalline Magnesium Aluminate Spinel Fabricated by Spark Plasma Sintering, Adv. Mater. 0(0) (2018) 1706283.

[34] A. Goldstein, A. Krell, Transparent Ceramics at 50: Progress Made and Further Prospects, J. Am. Ceram. Soc. (2016) 1-25.

22

[35] S. Alahraché, M. Deschamps, J. Lambert, M.R. Suchomel, D. De Sousa Meneses, G. Matzen, D. Massiot, E. Véron, M. Allix, Crystallization of Y_2O_3–Al_2O_3 Rich Glasses: Synthesis of YAG Glass-Ceramics, The Journal of Physical Chemistry C 115(42) (2011) 20499-20506.

[36] X. Ma, X. Li, J. Li, C. Genevois, B. Ma, A. Etienne, C. Wan, E. Véron, Z. Peng, M. Allix, Pressureless glass crystallization of transparent yttrium aluminum garnet-based nanoceramics, Nature Communications 9(1) (2018) 1175.

[37] A. Bertrand, J. Carreaud, S. Chenu, M. Allix, E. Véron, J.-R. Duclère, Y. Launay, T. Hayakawa, C. Genevois, F. Brisset, F. Célarié, P. Thomas, G. Delaizir, Scalable and Formable Tellurite-Based Transparent Ceramics for Near Infrared Applications, Advanced Optical Materials 4(10) (2016) 1482-1486.

[38] M. Allix, S. Alahrache, F. Fayon, M. Suchomel, F. Porcher, T. Cardinal, G. Matzen, Highly Transparent $BaAl_4O_7$ Polycrystalline Ceramic Obtained by Full Crystallization from Glass, Adv. Mater. 24(41) (2012) 5570-5575.

[39] Z. Xiao, S. Yu, Y. Li, S. Ruan, L.B. Kong, Q. Huang, Z. Huang, K. Zhou, H. Su, Z. Yao, W. Que, Y. Liu, T. Zhang, J. Wang, P. Liu, D. Shen, M. Allix, J. Zhang, D. Tang, Materials development and potential applications of transparent ceramics: A review, Materials Science and Engineering: R: Reports 139 (2020) 100518.

[40] L.B. Kong, Y.Z. Huang, W.X. Que, T.S. Zhang, S. Li, J. Zhang, Z.L. Dong, D.Y. Tang, Transparent Ceramics, Springer International Publishing2015.

[41] A. Krell, J. Klimke, T. Hutzler, Transparent compact ceramics: Inherent physical issues, Opt. Mater. 31(8) (2009) 1144-1150.

[42] G. Bonnefont, G. Fantozzi, S. Trombert, L. Bonneau, Fine-grained transparent $MgAl_2O_4$ spinel obtained by spark plasma sintering of commercially available nanopowders, Ceram. Int. 38(1) (2012) 131-140.

[43] G. Yu, W. Wang, C. Jiang, A facile approach towards fabrication and ultrabroad band emission properties of nickel ion-doped $ZnAl_2O_4$ transparent ceramics, Ceram. Int. 46(8, Part A) (2020) 10320-10324.

[44] A. Belyaev, L. Basyrova, V. Sysoev, M. Lelet, S. Balabanov, V. Kalganov, V. Mikhailovski, M. Baranov, E. Stepanidenko, V. Vitkin, O. Dymshits, P. Loiko, Microstructure, doping and optical properties of Co^{2+}:$ZnAl_2O_4$ transparent ceramics for saturable absorbers: Effect of the ZnF_2 sintering additive, J. Alloys Compd. 829 (2020) 154514.

[45] A.V. Belyaev, I.I. Evdokimov, V.V. Drobotenko, A.A. Sorokin, A new approach to producing transparent $ZnAl_2O_4$ ceramics, J. Eur. Ceram. Soc. 37(7) (2017) 2747-2751.

[46] X. Yong, F. Ping, Z. Baohua, G. Juan, Z. Lin, W. Xuehua, Optical properties of transparent $ZnAl_2O_4$ ceramics: A new transparent material prepared by spark plasma sintering, Mater. Lett. 123(0) (2014) 142-144.

[47] A. Goldstein, Y. Yeshurun, M. Vulfson, H. Kravits, Fabrication of Transparent Polycrystalline $ZnAl_2O_4$ – A New Optical Bulk Ceramic, J. Am. Ceram. Soc. 95(3) (2012) 879-882.

[48] A.V. Belyaev, M.I. Lelet, N.I. Kirillova, N.M. Khamaletdinova, M.S. Boldin, A.A. Murashov, S.S. Balabanov, Sol-gel synthesis and characterization of $ZnAl_2O_4$ powders for transparent ceramics, Ceram. Int. 45(4) (2019) 4835-4839.

[49] H.M. Rietveld, A profile refinement method for nuclear and magnetic structures, J. Appl. Crystallogr. 2(2) (1969) 65-71.

[50] V. Petricek, M. Dusek, L. Palatinus, Crystallographic Computing System JANA2006: General features, Zeitschrift für Kristallographie. Crystalline materials 229(5) (2014) 345-352.

[51] M. Rubat du Merac, H.-J. Kleebe, M.M. Müller, I.E. Reimanis, Fifty Years of Research and Development Coming to Fruition; Unraveling the Complex Interactions during

Processing of Transparent Magnesium Aluminate ($MgAl_2O_4$) Spinel, J. Am. Ceram. Soc. 96(11) (2013) 3341-3365.

[52] G.G.P. Van Gorkom, J.H. Haanstra, H. v. d. Boom, Infrared and Raman spectra of the spinel $ZnGa_2O_4$, Journal of Raman Spectroscopy 1(5) (1973) 513-519.

[53] R. Apetz, M.P.B. van Bruggen, Transparent alumina: A light-scattering model, J. Am. Ceram. Soc. 86(3) (2003) 480-486.

[54] Y. Abe, D.E. Clark, Determination of combined water in glasses by infrared spectroscopy, J. Mater. Sci. Lett. 9(2) (1990) 244-245.

[55] L. An, A. Ito, T. Goto, Highly transparent lutetium titanium oxide produced by spark plasma sintering, J. Eur. Ceram. Soc. 31(1) (2011) 237-240.

[56] K. Morita, B.-N. Kim, H. Yoshida, K. Hiraga, Y. Sakka, Distribution of carbon contamination in $MgAl_2O_4$ spinel occurring during spark-plasma-sintering (SPS) processing: I – Effect of heating rate and post-annealing, J. Eur. Ceram. Soc. 38(6) (2018) 2588-2595.

[57] Z. Galazka, D. Klimm, K. Irmscher, R. Uecker, M. Pietsch, R. Bertram, M. Naumann, M. Albrecht, A. Kwasniewski, R. Schewski, M. Bickermann, $MgGa_2O_4$ as a new wide bandgap transparent semiconducting oxide: growth and properties of bulk single crystals, physica status solidi (a) 212(7) (2015) 1455-1460.

[58] K. Morita, B.-N. Kim, H. Yoshida, K. Hiraga, Y. Sakka, Influence of pre- and post-annealing on discoloration of $MgAl_2O_4$ spinel fabricated by spark-plasma-sintering (SPS), J. Eur. Ceram. Soc. 36(12) (2016) 2961-2968.

[59] A. Bertrand, J. Carreaud, G. Delaizir, J.-R. Duclère, M. Colas, J. Cornette, M. Vandenhende, V. Couderc, P. Thomas, A Comprehensive Study of the Carbon Contamination in Tellurite Glasses and Glass-Ceramics Sintered by SPS, J. Am. Ceram. Soc. 97(1) (2014) 163-172.

[60] F.H. Hammoud, Mechanism of Carbon Contamination in Transparent $MgAl_2O_4$ and $Y_3Al_5O_{12}$ Ceramics Sintered by Spark Plasma Sintering, Ceramics 2 (2019).

[61] D. Gourier, A. Bessière, S.K. Sharma, L. Binet, B. Viana, N. Basavaraju, K.R. Priolkar, Origin of the visible light induced persistent luminescence of Cr^{3+}-doped zinc gallate, J. Phys. Chem. Solids 75(7) (2014) 826-837.

[62] W.W. Zhang, J.Y. Zhang, Z.Y. Chen, T.M. Wang, S.K. Zheng, Spectrum designation and effect of Al substitution on the luminescence of Cr^{3+} doped $ZnGa_2O_4$ nano-sized phosphors, J. Lumin. 130(10) (2010) 1738-1743.

[63] H.M. Kahan, Macfarla.Rm, Optical and Microwave Spectra of Cr^{3+} in the Spinel $ZnGa_2O_4$, J. Chem. Phys. 54(12) (1971) 5197-5205.

[64] W. Mikenda, A. Preisinger, N-lines in the luminescence spectra of Cr^{3+} doped spinels. (II) Origins of N-lines, J. Lumin. 26(1-2) (1981) 67-83.

[65] J. Derkosch, W. Mikenda, N-lines in the luminescence spectra of Cr^{3+} doped spinels. (IV) Excitation spectra, J. Lumin. 28(4) (1983) 431-441.

[66] W. Nie, F.M. Michelcalendini, C. Linares, G. Boulon, C. Daul, New results on optical properties and term energy calculations in Cr^{3+} doped $ZnAl_2O_4$., J. Lumin. 46(3) (1990) 177-190.

[67] G.G.P. van Gorkom, J.C.M. Henning, R.P. van Stapele, Optical Spectra of Cr^{3+} pairs irs in the Spinel $ZnGa_2O_4$, Physical Review B 8(3) (1973) 955-973.

[68] J. Derkosch, W. Mikenda, N-lines in the luminescence spectra of Cr3+-doped spinels: IV. Excitation spectra, J. Lumin. 28(4) (1983) 431-441.

[69] C.G. Walsh, J.F. Donegan, T.J. Glynn, G.P. Morgan, G.F. Imbusch, J.P. Remeika, Luminescence from β-Ga_2O_3: Cr^{3+}, J. Lumin. 40-41 (1988) 103-104.

[70] N. Basavaraju, K.R. Priolkar, A. Bessiere, S.K. Sharma, D. Gourier, L. Binet, B. Viana, S. Emura, Controlling disorder in the $ZnGa_2O_4$:Cr^{3+} persistent phosphor by Mg^{2+} substitution, PCCP 19(2) (2017) 1369-1377.

Supporting Information

First ZnGa$_2$O$_4$ Transparent Ceramics.

Claire Mével, Julie Carreaud, Gaëlle Delaizir, Jean-René Duclère, François Brisset, Julie Bourret, Pierre Carles, Cécile Genevois, Mathieu Allix, Sebastien Chenu*

Table SI-1: Atomic positions of ZnGa$_2$O$_4$ obtained from the room temperature Rietveld refinement of X-ray powder diffraction data (cell parameters: a= 8.32151(3)Å; space group: Fd-3m).

Atom	Site	x	y	z	Uiso (x100)	Occ.
Zn	8a	0.125	0.125	0.125	2.25(3)	1
Ga	16d	0.5	0.5	0.5	2.65(2)	1
O	32e	0.2591(1)	0.2591(1)	0.2591(1)	2.83(5)	1

.
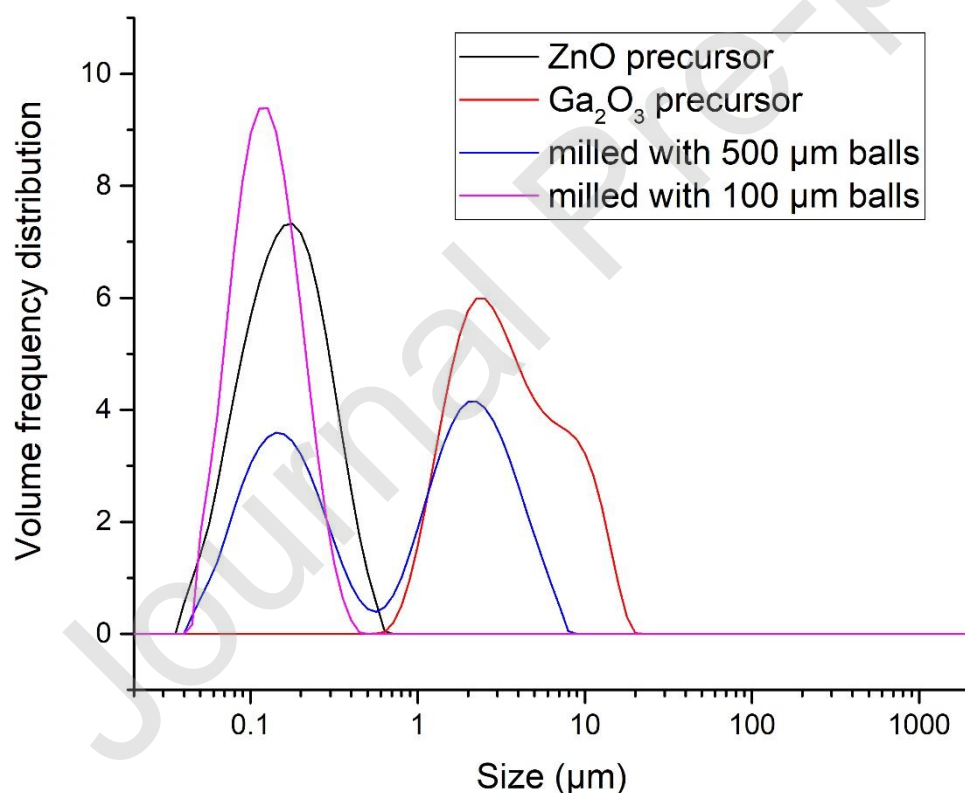
Figure SI-1: Particle size distribution of powder of precursors (ZnO and Ga$_2$O$_3$ with black and red curves respectively) and after ball milling process with zirconia balls with diameter of 500 μm (blue) and 100 μm (pink) during 20 minutes for each balls size.
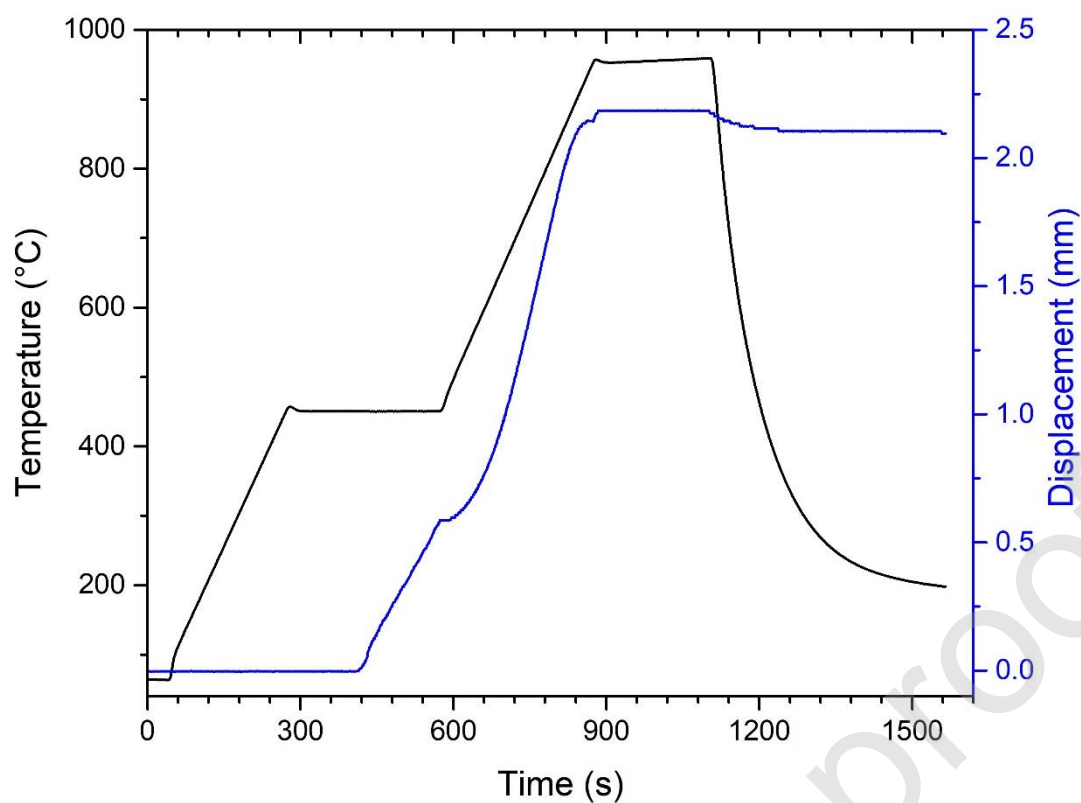
Figure SI-2: SPS sintering cycle and associated displacement.
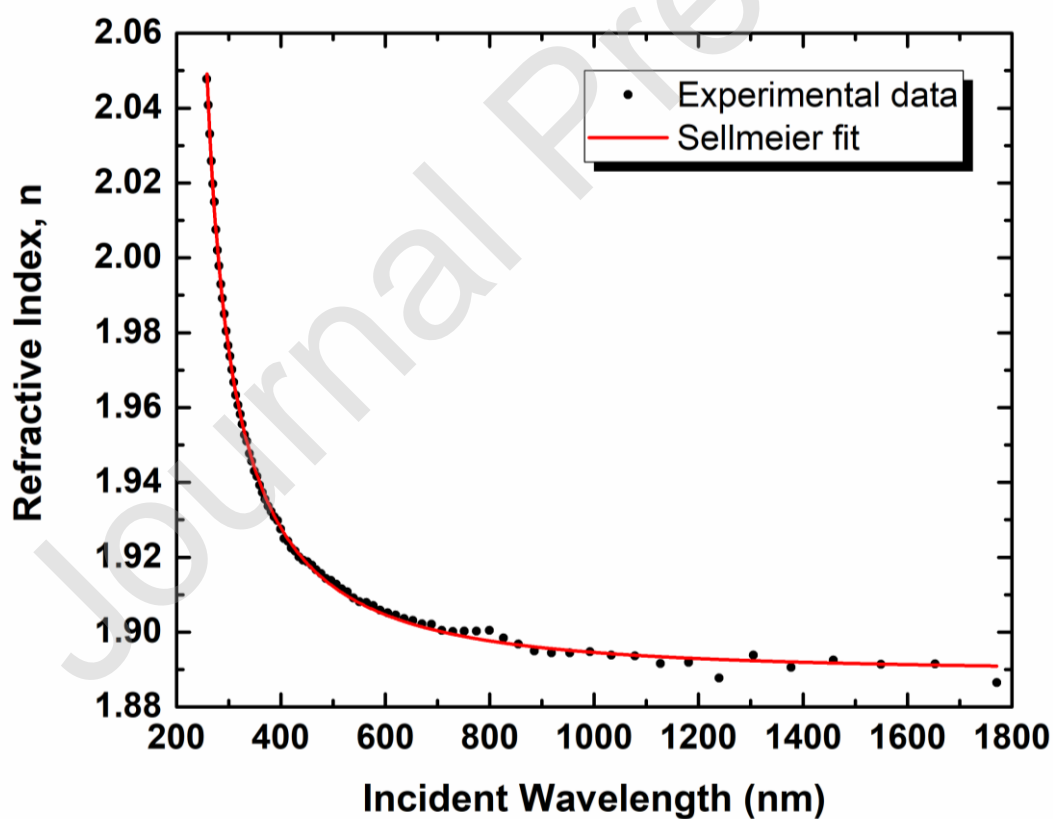
Figure SI-3: Chromatic dispersion of the linear refractive index of $ZnGa_2O_4$ transparent ceramic (black dots), measured by ellipsometry, and the corresponding Sellmeier fit (red curve). The r^2 parameter of the fit is equal to 0.9992, reflecting its good quality
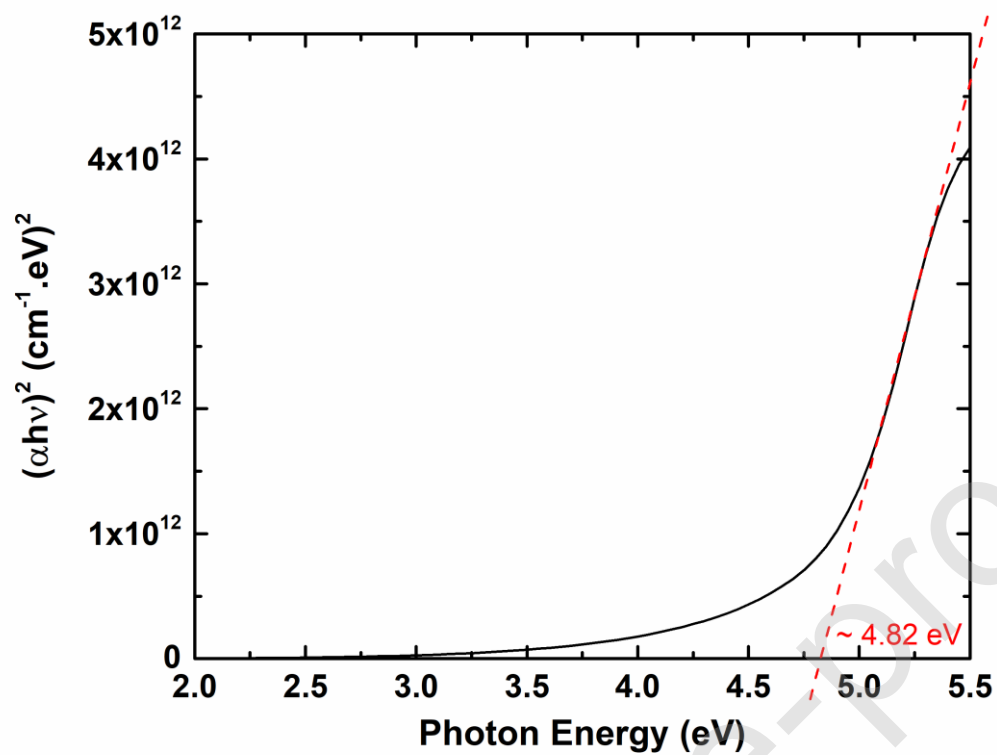
28

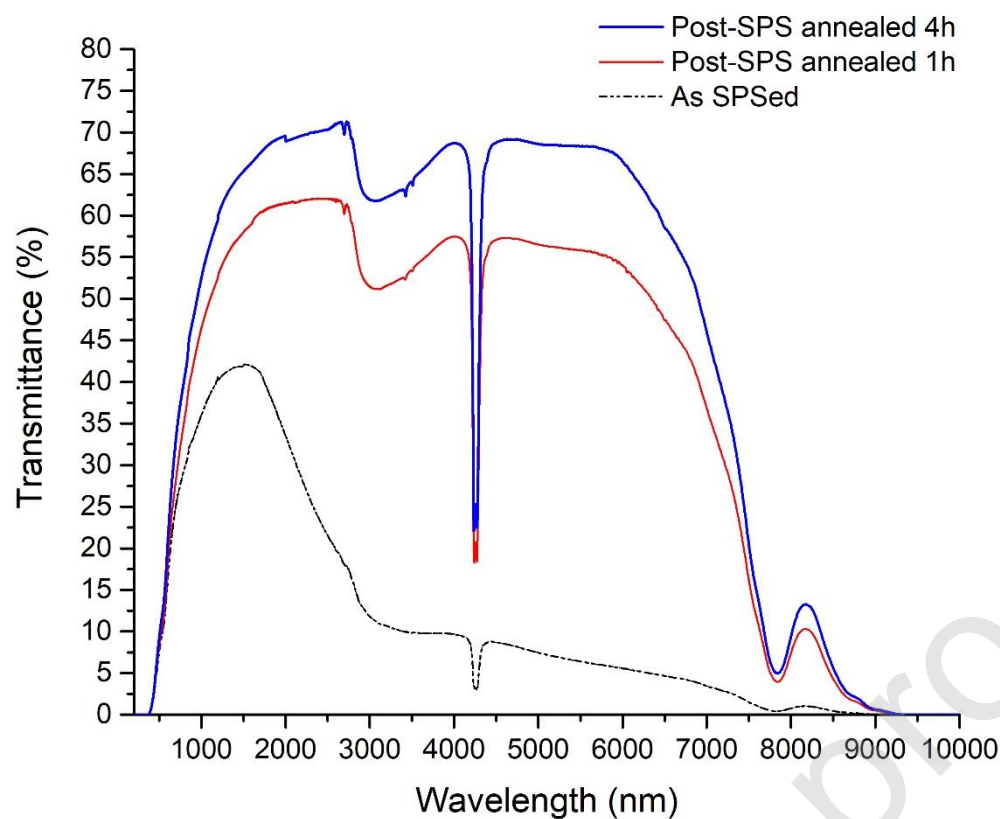**Figure SI-4**: Tauc plot ; representation for a direct transition allowed $(\alpha h\nu)^2 = f(h\nu)$, in the case of an undoped $ZnGa_2O_4$ transparent ceramic.

Figure SI-5: Optical transmittance spectra of Cr^{3+}-doped $ZnGa_2O_4$ transparent ceramic obtained by spark plasma sintering before and after thermal treatment in air at 800°C during 1 and 4 hours. (Thickness = 1 mm)

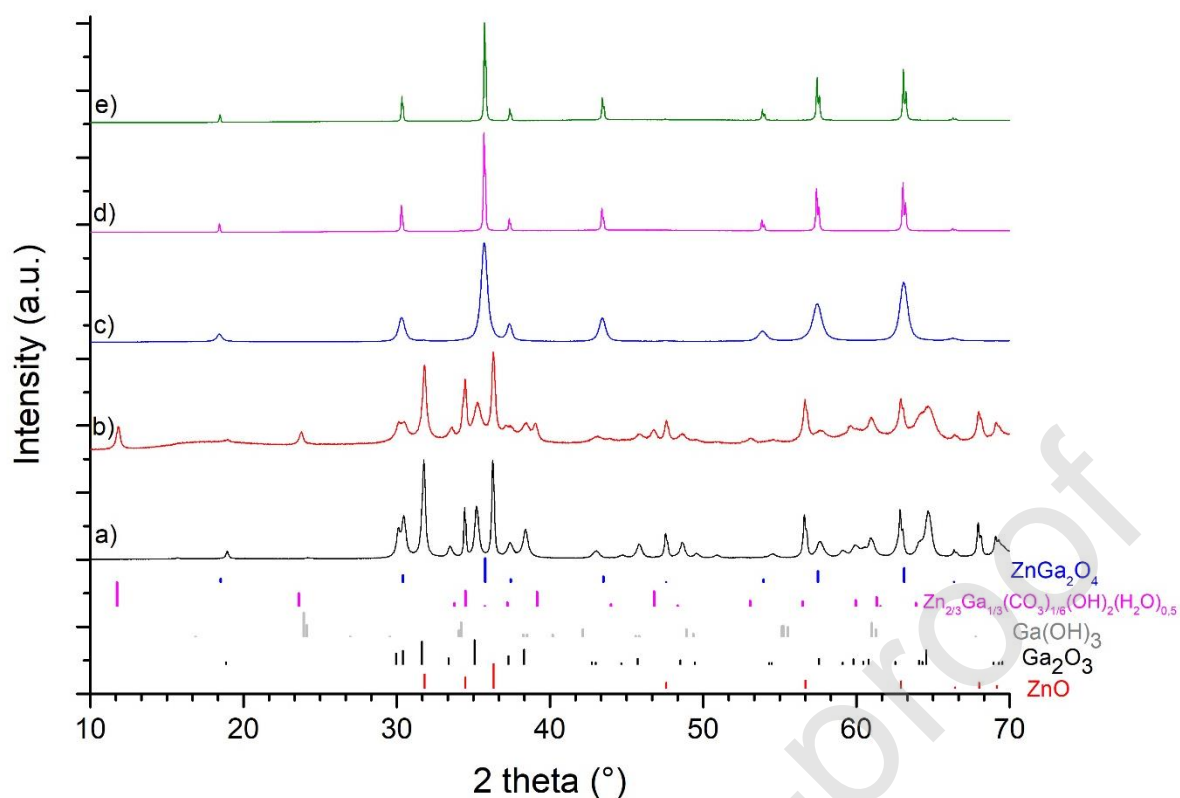**Figure SI-6**: X-ray powder diffraction patterns of the material at different steps of it elaboration: a) mixture of precursors (Ga_2O_3 and ZnO), b) after ball milling process, c) after heat treatment of 2h at 700°C, d) after SPS step, and e) after post-SPS air annealing during 4h at 800°C. The ZnO, Ga_2O_3, $Ga(OH)_3$, $Zn_{2/3}Ga_{1/3}(CO_3)_{1/6}(OH)_2(H_2O)_{0.5}$ and $ZnGa_2O_4$ indexations are indicated below.
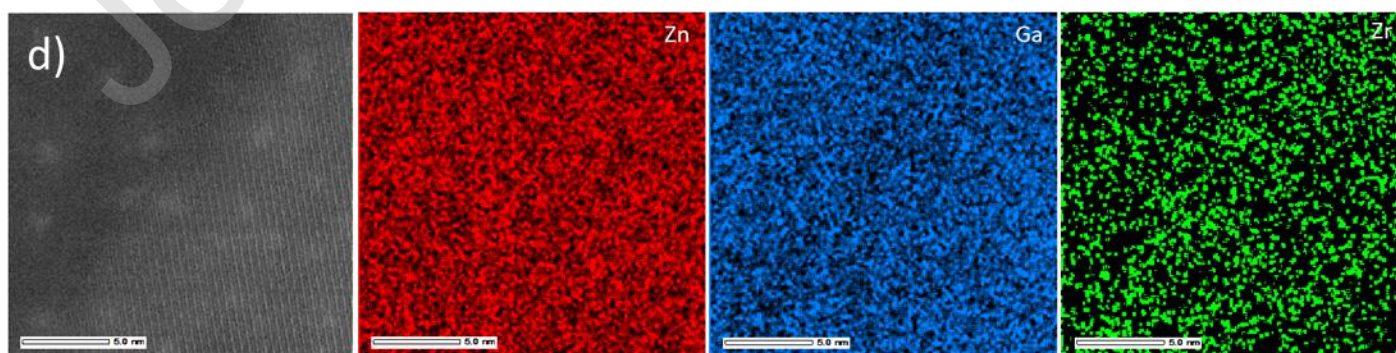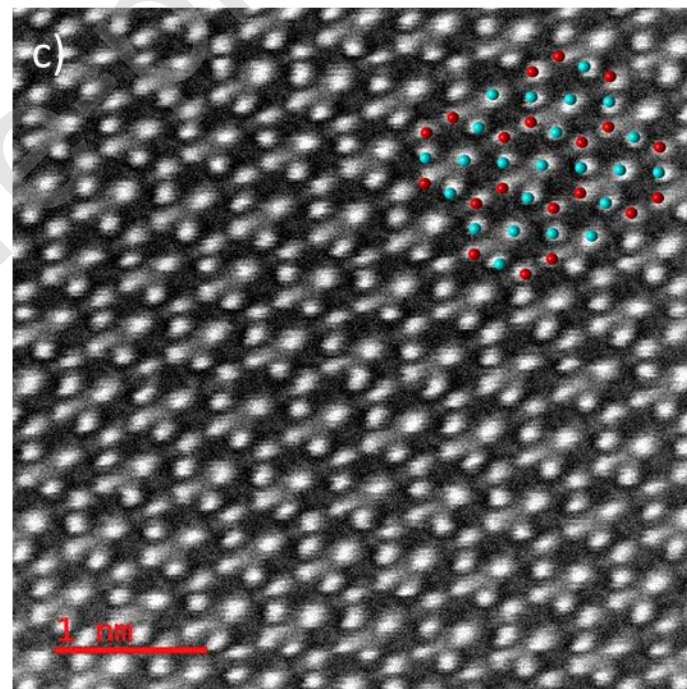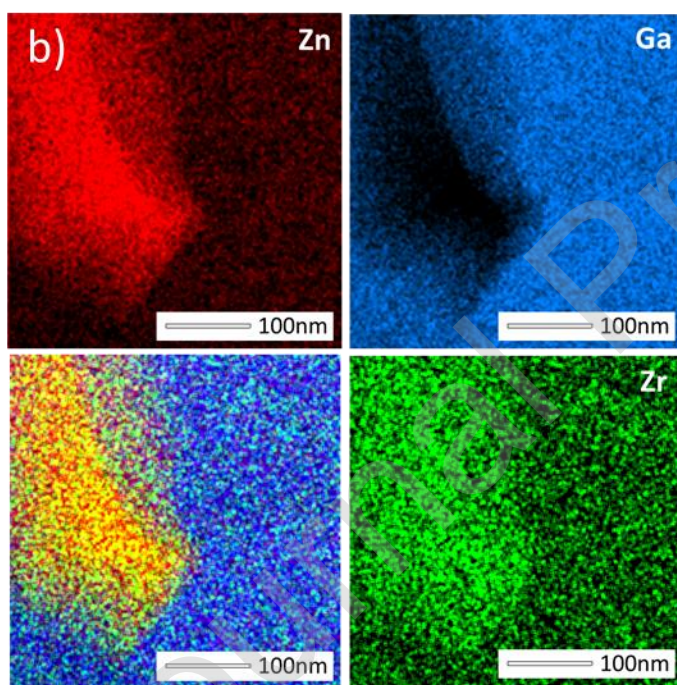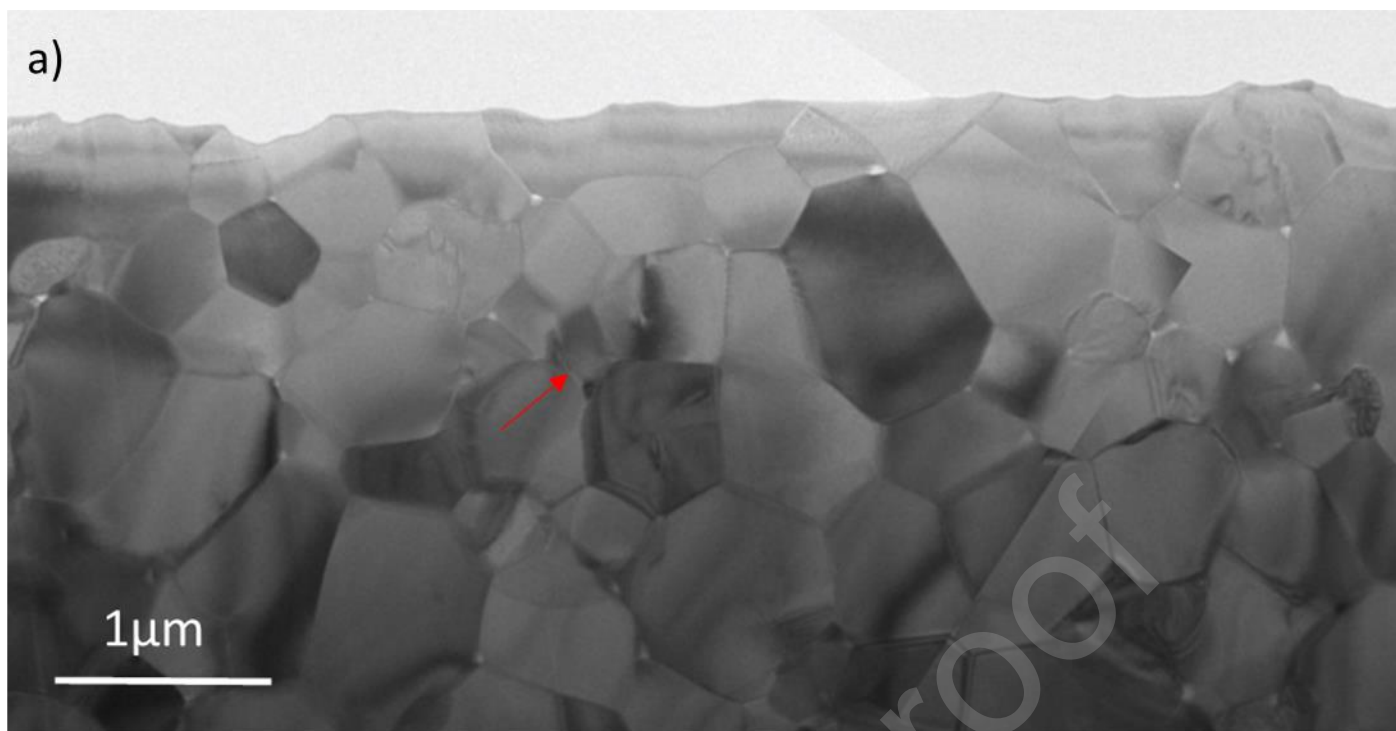
Figure SI-7: Cr^{3+}-doped $ZnGa_2O_4$ ceramic. (a) bright field TEM micrograph. (b) STEM-EDX elemental maps with associated Ga (blue), Zn (red) and Zr(green) of a secondary phase grain pointed by a red arrow on micrograph (a). (c) HRSTEM-HAADF of a single $ZnGa_2O_4$ grain with a [011] orientation. Imbedded, the atomic resolution image (blue for Ga and red for Zn atoms). (d) HRSTEM-HAADF of a thin grain boundary and STEM-EDX elemental maps with associated Ga (blue), Zn (red) and Zr(green) on the same area.